This is a repository copy of *Characterization of acoustic infrasound signals at Volcán de Fuego, Guatemala: a baseline for volcano monitoring*.

White Rose Research Online URL for this paper:
http://eprints.whiterose.ac.uk/168853/

Version: Published Version

Article:

frontiers
in Earth Science

Characterization of Acoustic Infrasound Signals at Volcán de Fuego, Guatemala: A Baseline for Volcano Monitoring

A. Diaz-Moreno[1]*, A. Roca[2], A. Lamur[3], B. H. Munkli[3], T. Ilanko[4], T. D. Pering[4], A. Pineda[5] and S. De Angelis[3]

[1]*School of Geography, Politics and Sociology, Newcastle University, Newcastle Upon Tyne, NW, United Kingdom,* [2]*Instituto Nacional de Sismología, Vulcanología, Meteorología e Hidrología, INSIVUMEH, Guatemala City, Guatemala,* [3]*School of Environmental Sciences, University of Liverpool, Liverpool, United Kingdom,* [4]*Department of Geography, University of Sheffield, Sheffield, United Kingdom,* [5]*Pineda Consulting and Services, Finca Xejuyu, Chimaltenango, Guatemala*

Monitoring volcanic unrest and understanding seismic and acoustic signals associated with eruptive activity is key to mitigate its impacts on population and infrastructure. On June 3, 2018, Volcán de Fuego, Guatemala, produced a violent eruption with very little warning. The paroxysmal phase of this event generated pyroclastic density currents (PDC) that impacted nearby settlements resulting in 169 fatalities, 256 missing, and nearly 13,000 permanently displaced from their homes. Since then, Volcán de Fuego has been instrumented with an extensive network of seismic and infrasound sensors. Infrasound is a new monitoring tool in Guatemala. A key step toward its effective use in volcano monitoring at Volcán de Fuego is establishing a baseline for the interpretation of the recorded signals. Here, we present the first comprehensive characterization of acoustic signals at Volcán de Fuego for the whole range of surface activity observed at the volcano. We use data collected during temporary deployments in 2018 and from the permanent infrasound network. Infrasound at Fuego is dominated by the occurrence of short-duration acoustic transients linked to both ash-rich and gas-rich explosions, at times associated with the generation of shock waves. The rich acoustic record at Fuego includes broadband and harmonic tremor, and episodes of chugging. We explore the occurrence of these signals in relation to visual observations of surface activity, and we investigate their source mechanisms within the shallow conduit system. This study provides a reference for the interpretation of acoustic signals at Volcán de Fuego and a baseline for real-time monitoring of its eruptive activity using infrasound data. Our results suggest that changes in the style of activity and morphology of the summit crater are reflected in the acoustic signature of eruption; as such our study provides a reference for the interpretation of acoustic signals at Volcán de Fuego and a baseline for real-time monitoring of its eruptive activity using infrasound.

Keywords: acoustic infrasound, Volcán de Fuego, monitoring, Strombolian activity, paroxysmal activity

1. INTRODUCTION

Effective monitoring strategies are a key aspect of hazard mitigation near volcanoes (Tilling, 2008). Real-time, multi-parameter, monitoring of volcanoes is key to reduce the impact of eruptions on communities and infrastructure (McNutt et al., 2015; Pallister and McNutt, 2015; Ripepe and Marchetti, 2019). At present, less than half of the world's active volcanoes with Holocene eruptions in historical times, that is in the past 10,000 years, are instrumentally monitored (McNutt et al., 2015). At many volcanoes, resources devoted to developing monitoring programs have traditionally been scarce, leading to severe impacts of eruptions on population and infrastructure. A recent example is Volcán de Fuego, Guatemala, where an eruption with associated pyroclastic flows occurred on June 3, 2018 causing 169 confirmed casualties, 256 missing, severe damage to population centers and infrastructure, and associated economic losses (Global Volcanism Program, 2018c). Interest in understanding the eruptive behavior of Volcán de Fuego, sparkled after a sub-plinian event in 1974 (Rose et al., 1978; Chesner and Rose, 1984; Yuan et al., 1984; Berlo et al., 2012). Early monitoring efforts consisted of visual and field observations; short-term multi-parameter deployments including gas, seismic and infrasound measurements became increasingly common through the past decade (e.g., Lyons et al., 2010; Lyons and Waite, 2011; Nadeau et al., 2011; Brill et al., 2018; Naismith et al., 2019). Before the eruption on June 3, 2018, the permanent network operated by Instituto Nacional de Sismología, Vulcanología, Meteorología e Hidrología (INSIVUMEH) consisted of a single seismic station located 7.5 km from the active vent streaming data in real-time to INSIVUMEH headquarters. However, data dropouts were frequent and until 2018 continuous seismic data were not archived. Since June 2018, the monitoring capabilities at Volcán de Fuego have been greatly enhanced; at the time of this writing, the monitoring network operated by INSIVUMEH consists of three 6-channel seismo-acoustic arrays (each including one 3-component broadband seismometer and three infrasound microphones), three 3-component broadband seismic stations, and one 6-channel infrasound array deployed at distances of 3–15 km from the vent, transmitting data in real-time to the INSIVUMEH headquarters in Guatemala City.

Among the different techniques used in volcano observatories, seismology and infrasound continue to offer unmatched temporal resolution for near real-time volcano monitoring (Brill et al., 2018; Marchetti et al., 2019). In recent times, acoustic infrasound has emerged as an increasingly popular tool for volcano remote sensing. The term infrasound identifies atmospheric acoustic waves with frequencies typically <20 Hz, below the audible range of humans. Volcanoes are prolific radiators of infrasound, generated by eruptive processes that cause rapid acceleration of the atmospheric mass (Garcés et al., 2013); these low-frequency acoustic waves can be detected at distances of up to several thousands of kilometers from their source lending themselves to volcano monitoring at different scales, from local to global (Matoza et al., 2018). The use of infrasound for regional and local volcano monitoring, with applications in volcano early warning, has become increasingly popular (Kamo et al., 1994; Garcés et al., 2008; Fee et al., 2010b; De Angelis et al., 2012; De Angelis et al., 2019; Ripepe et al., 2018). Different configurations for deployment of infrasound microphones generate different products and therefore, sensors are generally installed according to specific scopes (Matoza et al., 2019b). Local distributed networks of individual microphones are ideal for locating and characterizing eruptive activity offering potential to assess open conduit volcanic emissions in real- or near real-time (Cannata et al., 2009a; Johnson and Ripepe, 2011; Fee and Matoza, 2013; De Angelis et al., 2019; Iezzi et al., 2019). On the other hand, arrays, that is clusters of three or more tightly spaced sensors, are commonly used to detect and locate low-amplitude signals (i.e., tremor, lahars, Johnson and Palma, 2015). Arrays can also detect and identify volcanic infrasound transients at global and regional distances contributing to monitoring of non-accessible remote volcanoes (Walker et al., 2010; Lyons et al., 2020). Co-location of seismic and acoustic sensors can provide additional insights into the dynamics of volcanic activity where a more extensive monitoring network is not available (Nishida and Ichihara, 2016; Matoza et al., 2019a).

Volcán de Fuego has hosted several seismo-acoustic experiments since 2005. These campaigns have shed light into the dynamics of the volcanic system, from the occurrence of cycles of activity to the source mechanisms of individual explosions. Observations during 2005–2007 including seismo-acoustic deployments led to the first comprehensive study of eruption dynamics at Volcán de Fuego (Lyons et al., 2010), a milestone for future experiments. Two temporary seismo-acoustic deployments in January 2008 and 2009 gathered valuable data that further contributed to our knowledge on the occurrence of very-long period seismicity (Lyons and Waite, 2011; Waite et al., 2013), SO2 imaging (Nadeau et al., 2011), tilt changes and ultra-long-period events (Lyons et al., 2012), and seismo-acoustic tremor (Lyons et al., 2013) and allowed modeling of the processes that control eruption dynamics at Fuego. Recent experiments, conducted in January 2012, included seismo-acoustic deployments, collection of thermal infrared imagery, and gas and tilt measurements; some of the data collected in 2012 were recently used to define a baseline for seismic monitoring at the volcano (Brill et al., 2018). We conducted temporary deployments during 18–23 May 2018 and 26 November–3 December 2018 to gather infrasound data from activity at Volcán de Fuego. A new geophysical permanent monitoring network was installed at the volcano in the aftermath of the June 2018 eruption, including six new seismic stations and four infrasound arrays (**Figure 1**).

The scope of this manuscript is to present an overview of the range of infrasound signals associated with recent eruptive activity using data from the above mentioned temporary deployments, and link them to surface activity observed at the volcano. We envision that this work will serve as an initial baseline to inform infrasound monitoring of Volcán de Fuego.
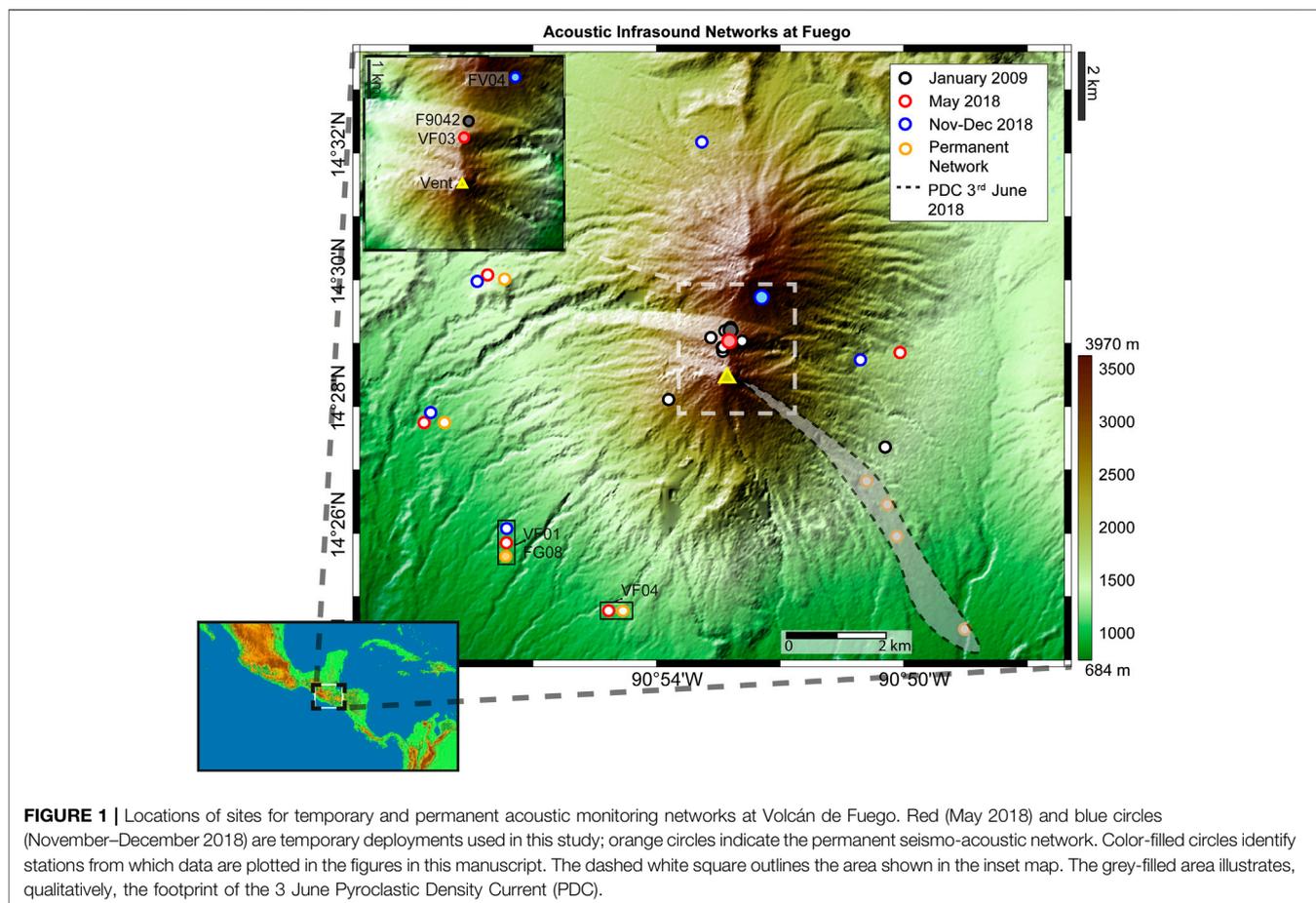
FIGURE 1 | Locations of sites for temporary and permanent acoustic monitoring networks at Volcán de Fuego. Red (May 2018) and blue circles (November–December 2018) are temporary deployments used in this study; orange circles indicate the permanent seismo-acoustic network. Color-filled circles identify stations from which data are plotted in the figures in this manuscript. The dashed white square outlines the area shown in the inset map. The grey-filled area illustrates, qualitatively, the footprint of the 3 June Pyroclastic Density Current (PDC).
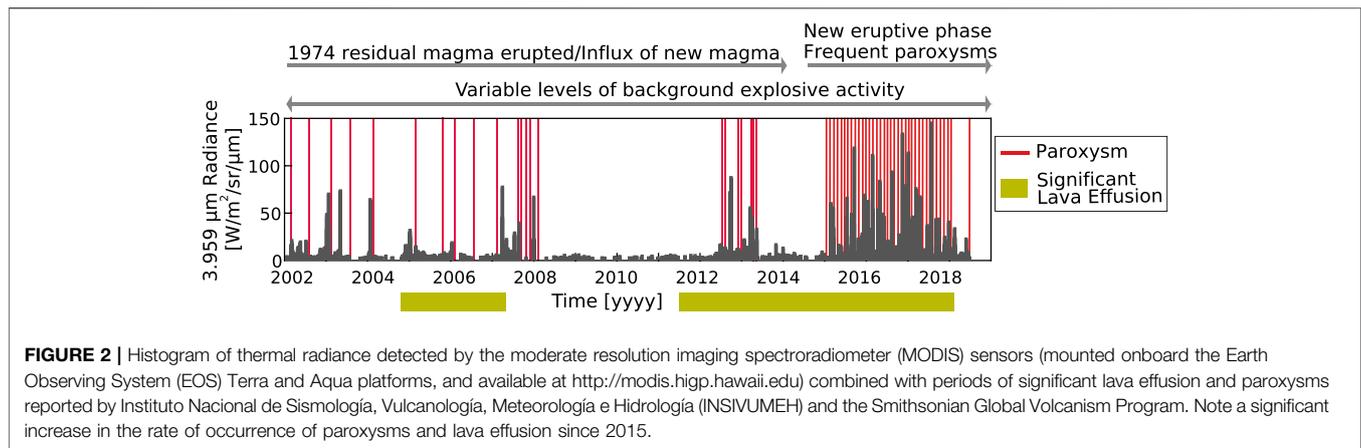
2. VOLCÁN DE FUEGO

Volcán de Fuego is one of the most active volcanoes in central and south America (Wolf-Escobar, 2013). It is a basaltic strato-volcano standing nearly 3,800 m above sea level in the Central America Volcanic Arc (14.47°N, 90.88°W), and marks the southernmost active part of the four-vent Fuego-Acatenango volcanic complex (Guatemala), which has been migrating southwards since 230 ka (Chesner and Rose, 1984). While the main growth period of this complex is dated 84 ka (Vallance and Iverson, 2015), volcanic activity at the current vent may have begun 13 ka (Martin and Rose, 1981). Bulk rock data collected at Meseta and Volcán de Fuego showed fractionation of plagioclase, olivine, clinopyroxene, and magnetite consistent with a high-aluminium basaltic composition (51% SiO2; Chesner and Rose, 1984). Moreover, melt inclusions in erupted olivine indicate that Fuego's magmas, like many other arc basalts and basaltic andesites, contain dissolved H_2Oconcentrations between 2.1 and 6.1 wt% (Sisson and Layne, 1993; Roggensack, 2001). This high volatile content is thought to influence eruptive behavior during open-vent periods. Reports of activity since 1954 include at least 60 eruptions characterized by Volcanic Explosivity Index (VEI) 2 with associated pyroclastic flows, and interspersed with frequent Strombolian activity (Rose et al., 1978; Berlo et al., 2012; Naismith et al., 2019). During the last century, three sub-Plinian

events have occurred: i) a VEI 4 eruption in January 1932 that generated a >5 km a.s.l. plume and modified the vent's morphology leaving ash deposits across Guatemala (Deger, 1932; Naismith et al., 2019); ii) a VEI 4 eruption in October 1974, which included four major stages producing lava flows, ash fall, pyroclastic flows and lahars, forced the mobilization of population, and caused important damage on the agriculture (Rose et al., 1978); and iii) the recent eruption on June 3, 2018 (Global Volcanism Program, 2018c).

2.1. Long-Term Evolution of Eruptive Activity

Activity at Volcán de Fuego since 1974 can be summarized as long quiescence until 1999, followed by the reactivation of eruptive processes that remained nearly continuous until present. Persistent activity at Fuego is characterized by extended periods of lava effusion, frequent but moderate explosions, and episodes of paroxysmal activity. Paroxysms at Volcán de Fuego are defined as eruptive phases that start with the onset of energetic explosive activity rapidly increasing in rates and intensity leading to large sustained emission of pyroclastic material, which persists for 24–48 h (e.g., Lyons et al., 2010). Indeed, the rate of occurrence of paroxysms has greatly increased since late 2014 (**Figure 2**).

The 1974 eruption of Fuego had an estimated VEI = 4, generated sustained ash columns reaching a height of over

FIGURE 2 | Histogram of thermal radiance detected by the moderate resolution imaging spectroradiometer (MODIS) sensors (mounted onboard the Earth Observing System (EOS) Terra and Aqua platforms, and available at http://modis.higp.hawaii.edu) combined with periods of significant lava effusion and paroxysms reported by Instituto Nacional de Sismología, Vulcanología, Meteorología e Hidrología (INSIVUMEH) and the Smithsonian Global Volcanism Program. Note a significant increase in the rate of occurrence of paroxysms and lava effusion since 2015.

7 km above the vent, and produced Pyroclastic Density Currents (PDC) with a run-out of 8 km. The eruption, composed of four major events, lasted 14 days and led to substantial damage in villages up to 40 km from the summit mainly caused by PDCs and ashfall (Roggensack, 2001; Naismith et al., 2019). Many studies link this event to the ascent of magma from a lens-shaped vertical body located at about 8 km depth connected to a larger, deeper, storage region, with some suggesting the presence of an even deeper reservoir near the crust-mantle boundary (Rose et al., 1978; Martin and Rose, 1981; Chesner and Rose, 1984; Roggensack, 2001). Nearly 2 decades of quiescence followed the 1974 eruption.

In 1999 a new period of unrest began, characterized by periods of lava effusion accompanied by Strombolian explosions and episodic paroxysmal activity. **Figure 2** illustrates this behavior from thermal radiance data since 2002 plotted alongside reported paroxysms and periods of significant lava effusion. Note that moderate resolution imaging spectroradiometer (MODIS) pixel resolution varies from 250 m to 1 km, and thus, the thermal radiance data showed in **Figure 2** do not allow separating activity at the summit from that occurring on the upper flanks of the volcanic edifice. Lack of data resolution (flank activity vs. summit activity) does not influence interpretation of the activity over this 20-years scale. Current resolution does not allow us to establish which thermal anomalies are caused by active lava flows or which by significant explosions. Qualitatively, both lava flows and large explosions increase contemporaneously. However additional data will be needed to accurately answer this question (i.e., better satellite resolution images, visual data from field). During 1999–2003, erupted products were similar in composition to 1974 although more differentiated, that is showing more evolved melt inclusions. This activity was interpreted as linked to remaining magma from 1974 stored at shallow depths and being pushed out by the ascent of a new batch of magma from depth. Berlo et al. (2012) suggested that paroxysmal activity would continue in the years to come, fueled by renewed supply of fresh magma. Intermittent activity reported throughout the period 2000–2014 confirmed a new phase of volcanic activity, dominated by relatively frequent explosive

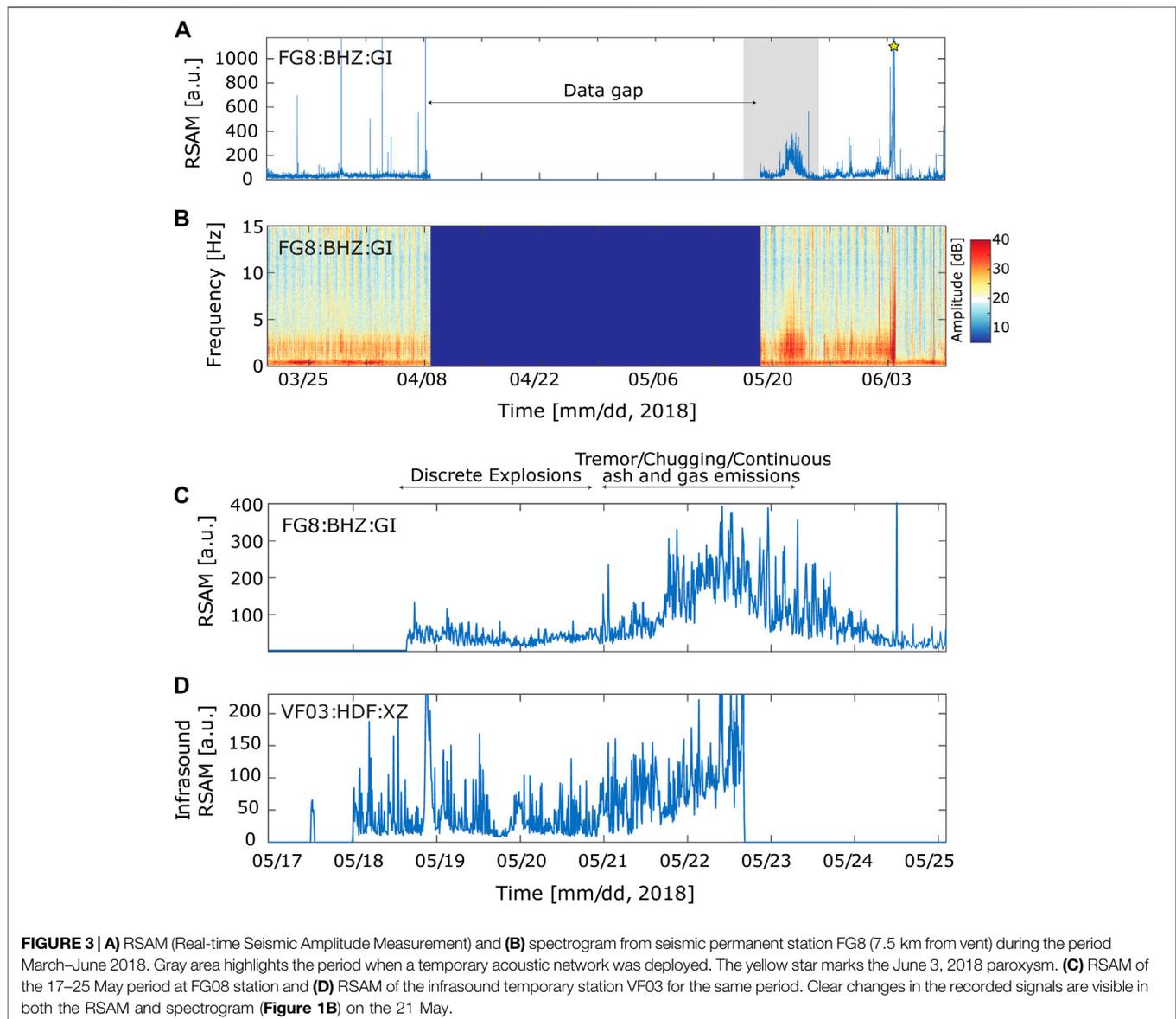eruptions and effusive activity (Lyons et al., 2010; Naismith et al., 2019).

Starting in early 2015 activity was characterized by more regular cycles of lava effusion (5–10 days) accompanied by frequent Strombolian explosions, preceding (1–2 days) episodes of more vigorous and sustained explosive activity, followed by a decrease in activity (Naismith et al., 2019). Since 2015 paroxysms at Volcán de Fuego have occurred more frequently until the event on June 3, 2018 (**Figure 1**). During this eruptive episode intense degassing and sustained ash plumes rising up to 3 km above the vent were followed by PDCs. The pyroclastic flows, with a run-out of more than 11 km along the Las Lajas valley, destroyed part of La Reunion Resort, the Las Lajas bridge on the National Route (RN) 14, and buried the village of San Miguel Los Lotes. Official figures report at least 169 casualties, 256 people missing, and nearly 13,000 people evacuated (Global Volcanism Program, 2018c; Ferrés, 2019; Naismith et al., 2019; Pardini et al., 2019). Furthermore, the ash and pyroclastic deposits during the rainy season fueled several lahars in the following months (Global Volcanism Program, 2018c).

3. DATA AND RECENT ACTIVITY

Here, we take advantage of data collected during two campaigns that were conducted in 18–23 May and 26 November - December 3, 2018 (**Figure 1**).

3.1. May 2018 Deployment

Activity reports from INSIVUMEH describe activity during the period 16–22 May 2018 as characterized by frequent explosions (5–8 per hour), some of which injected ash at elevations of up to 1 km above the vent. The explosive activity caused rumbling sounds and produced shock waves (pressure perturbations that move faster than the speed of sound in the atmosphere) locally referred to as cañonazos. The loud noise produced by shock waves was frequently heard as far as 30 km from the volcano (Global Volcanism Program, 2018a). In May 2018 we deployed a temporary network (18–23 May 2018) of six infrasound sensors

FIGURE 3 | A) RSAM (Real-time Seismic Amplitude Measurement) and **(B)** spectrogram from seismic permanent station FG8 (7.5 km from vent) during the period March–June 2018. Gray area highlights the period when a temporary acoustic network was deployed. The yellow star marks the June 3, 2018 paroxysm. **(C)** RSAM of the 17–25 May period at FG08 station and **(D)** RSAM of the infrasound temporary station VF03 for the same period. Clear changes in the recorded signals are visible in both the RSAM and spectrogram (**Figure 1B**) on the 21 May.
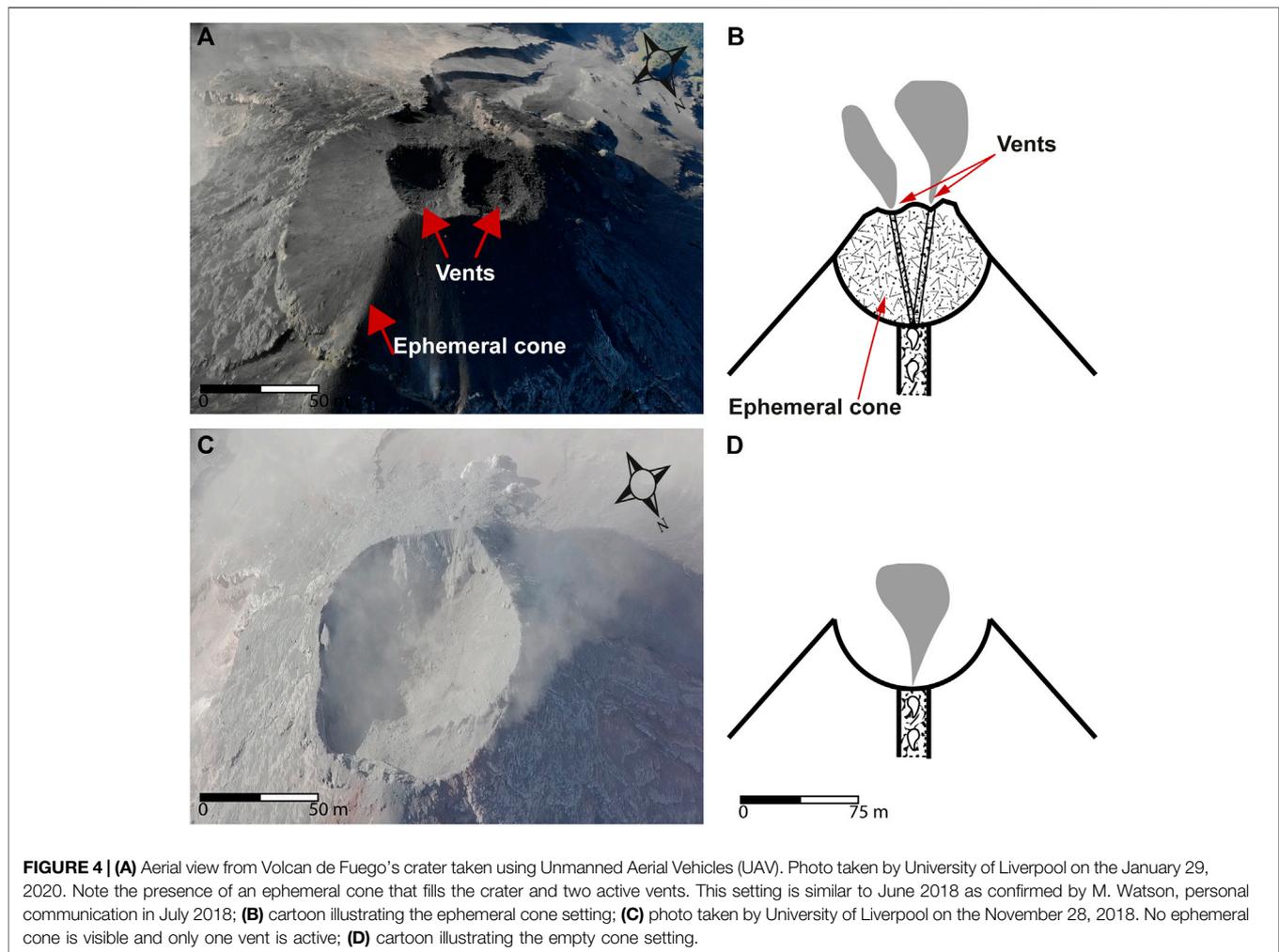
(Chaparral M60-UHP), located between 1 and 9 km from the active vent. The sensors have a sensitivity of 9 mV/Pa, flat response between 0.03 and 245 Hz, and a full-scale range of 2,000 Pa. Data were sampled at 100 Hz with 24-bit resolution using DiGOS DATA-CUBE digitizers. During the deployment eruptive activity shifted from discrete and energetic gas-rich explosions to Strombolian-type explosions, then to sustained ash and gas emissions accompanied by quasi-continuous acoustic tremor on 21–23 May. This change is visible as an increase in amplitude in both RSAM (Real-time seismic amplitude measurement) and spectrogram from the only broadband seismic station available at the time, and one of the temporary infrasound sensors illustrated in **Figure 3**. Data gathered from this campaign show a wide range of infrasound waveforms, some of which resemble previously reported signals at Volcán de Fuego (Lyons et al., 2010; Lyons, 2011) including

gas- and ash-rich explosions, shock waves, harmonic, and broadband tremor. We also recorded periods of strong chugging, described in the literature (e.g., Johnson and Lees, 2000; Lees and Ruiz, 2008) as a particular instance of quasi-periodic harmonic tremor. Chugging was observed at Volcán de Fuego for the first time by Lyons et al. (2010). During this period INSIVUMEH reported the presence of two active vents within the summit area at Fuego (G. Chigna, personal communication July 2018). This configuration is typical at Fuego when the crater is filled by lava and the two vents are frequently observed to produce distinct types of explosions, one gas-rich and another ash-rich (**Figure 4**).

3.2. November-December 2018 Deployment
During November-December 2018 — soon after the most recent paroxysm in mid-November 2018 — INSIVUMEH reported

FIGURE 4 | (A) Aerial view from Volcan de Fuego's crater taken using Unmanned Aerial Vehicles (UAV). Photo taken by University of Liverpool on the January 29, 2020. Note the presence of an ephemeral cone that fills the crater and two active vents. This setting is similar to June 2018 as confirmed by M. Watson, personal communication in July 2018; **(B)** cartoon illustrating the ephemeral cone setting; **(C)** photo taken by University of Liverpool on the November 28, 2018. No ephemeral cone is visible and only one vent is active; **(D)** cartoon illustrating the empty cone setting.

moderate to strong explosions (10–15 per hour), some of them accompanied by audible noise heard at 20–25 km from the vent, and ash plumes rising up to 1.3 km above the summit during 21–27 November (Global Volcanism Program, 2018b). In the period between 26 November and December 3, 2018 we deployed a temporary network, consisting of six acoustic infrasound sensors (5 Chaparral M60-UHP and one IST-2018 differential microphone). The IST-2018 sensor has a sensitivity of 19.8 mV/Pa, corner frequency of 7 mHz, and full-scale range of +/−230 Pa (Grangeon and Lesage, 2019). Data were sampled at 100 Hz with 24-bit resolution using DiGOS DATA-CUBE digitizer. The activity recorded consisted of discrete explosions with variable intensity and gas and ash content, interspersed with periods of persistent degassing lasting up to 2 h (**Supplementary Material SM1**). Unmanned Aerial Vehicle (UAV) footage recorded during this deployment shows an empty crater with only one clearly visible active vent (**Figure 4**).

3.3. Permanent Network

A permanent seismo-acoustic network was installed at Volcán de Fuego after the June 2018 eruption. The network consists of three 6-channel seismo-acoustic arrays (one 3-component broadband

seismometer and three infrasound microphones), three 3-channel broadband seismic stations, and one 6-channel infrasound array deployed at distances between 3 and 15 km from the vent. All stations were installed between July 30, 2018 and April 2, 2019. Data are telemetered in real-time to the INSIVUMEH headquarters in Guatemala City. The most notable activity recorded since the first deployment in July 2018 was one paroxysm on 17–18 November 2018 — leading to the evacuation of 3,925 people from nearby villages — and vigorous lava effusion during March-April 2019.

4. INFRASOUND SIGNALS AT VOLCÁN DE FUEGO

Locally recorded (<10 km from source) volcanic infrasound at Volcán de Fuego ranges from impulsive transients to tremor-like sustained waveforms, with a number of other intermediate types (McNutt et al., 2015). The impulsive transients, characterized by short duration (5–15 s) and sharp onsets (**Figures 4A–C**), are commonly generated by short-duration explosive sources. These signals feature a rapid compression followed by a rarefaction

phase with a nearly symmetrical shape (e.g., 5 d, g, and **Supplementary Material SM2**), which is indicative of a flow rate source time function symmetrically distributed in time around a peak value (Brogi et al., 2018; De Angelis et al., 2019). In other instances waveforms are non-symmetrical, exhibiting rapid compression onsets followed by rarefaction phases with reduced amplitudes (e.g., 5 a); waveform asymmetry may represent either a non-symmetrical flow rate source function, or reflect a shock-type source mechanism similar to blast waves produced by chemical explosions (Marchetti et al., 2013; Brogi et al., 2018). Typically, blast waves can be separated from other explosion mechanisms due to their characteristic appearance and much larger peak amplitudes, of the order of several hundreds of Pa at few hundred meters from the source. Diversity in the characteristics of infrasound signals reflects variety in their source mechanisms, and may provide additional clues on whether explosions are gas- or tephra-rich (Matoza et al., 2014). Observational evidence from our campaigns and continuous visual monitoring of activity at Volcán de Fuego by INSIVUMEH suggests that waveforms featuring impulsive onsets followed by several additional pulses, or by a prolonged coda (e.g., 5 g), are frequently associated to the generation of tephra-rich plumes. Generally, longer duration signals reflect sustained source caused either by multiple short pulses or longer duration pulses. Waveform and frequency content depend also on the ash content in the plume, turbulence in the plume and other factors still to be studied. At the other end of the spectrum of infrasound signals we find non-impulsive, low-amplitude, and long-duration waveforms known as acoustic tremor. These events — considered one of the best precursors of an eruption (Fee and Garcés, 2007) — are typical at many other volcanoes and result from processes within the magmatic fluid (Fee et al., 2010a). Acoustic tremor can last from minutes to days and is frequently recorded along with its seismic counterpart. It is classified into different categories according to its spectral characteristics, including broadband, and harmonic tremor (Lyons et al., 2013). In this section, we describe the near-field acoustic fingerprint of volcanic activity at Volcán de Fuego during 2018 and draw a comparison with previous observations (Lyons, 2011), which shows similar events (**Supplementary Material SM3**).

4.1. Strombolian Explosive Activity

Strombolian activity generally occurs in silica-poor, low-viscosity magmas (e.g., Parfitt and Wilson, 1995; Taddeucci et al., 2015), similar to the composition at Volcán de Fuego (Chesner and Rose, 1984; Berlo et al., 2012). It commonly manifests as discrete bursts associated with the rise of gas slugs through the magmatic column, producing variable amounts of tephra and pyroclasts (Taddeucci et al., 2015). The overpressures during such explosions at Volcán de Fuego suggest a more complex mechanism than a simple slug burst through consistently low viscosity magma. In fact, previous works by Lyons (2011) and Nadeau et al. (2011) describe the presence of a viscous magma plug at the top of the magma column, able to retain overpressure prior to brittle failure, which is responsible for explosive activity. This model acknowledges the role of a crystal mush or plug at the top of the column proposed by other authors (Suckale et al., 2016; Barth et al., 2019; Girona et al., 2019),
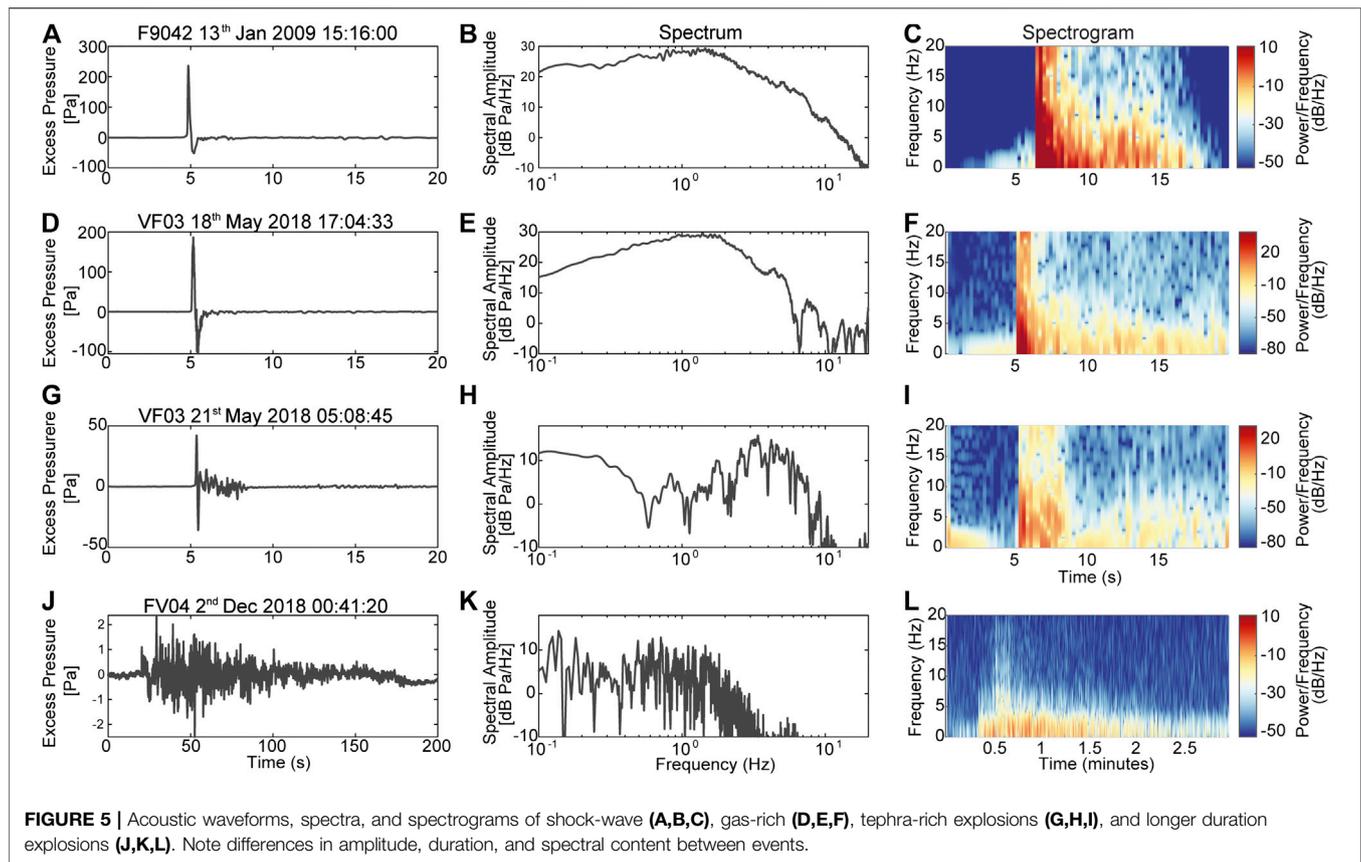
highlighting its importance in defining explosion dynamics. At Volcán de Fuego, these discrete explosions together with longer duration signals associated to non-explosive activity (**Supplementary Material SM2 d**), represent the dominant background through the past decade. Explosive activity generally accompanies periods of active lava effusion and precedes the nearly-periodic occurrence of violent paroxysms.

Acoustic records of explosive activity at Volcán de Fuego exhibit differences in amplitude, frequency content, and coda duration. According to these observations infrasound waveforms can be grouped into three main categories: i) Gas-rich explosions; ii) Tephra-rich explosions and iii) Long duration events. **Figure 5** shows infrasound waveforms, spectra, and spectrograms of all three types of events. Note that despite the common impulsive symmetric onset for both gas- and tephra-rich explosions, these types of events clearly differ in coda length, signal amplitude, and spectral content; gas-rich events generally deliver acoustic energy at higher frequencies, and feature more energetic signals and shorter duration coda.

Gas-Rich Explosions

Gas-rich explosions are short-duration (order of 2–3 s) acoustic transients with variable peak amplitudes (**Figure 5B** and **Supplementary Material SM2 b**; Johnson, 2003; Fee and Matoza, 2013). Examples of these type of events have been reported at multiple volcanoes worldwide including Stromboli (Ripepe and Marchetti, 2002), Etna (Cannata et al., 2009b; Marchetti et al., 2009), and Yasur (Marchetti et al., 2013). Visual observations, conducted in the field by the authors during the November 2018 campaign, confirmed that gas-rich explosions produced light gray plumes formed from a single initial pulse rising between 500–1,500 m above the vent. Some gas-rich bursts are driven by sufficient overpressure to generate shock waves; the associated waveforms are characterized by a sharp compressive onset followed by a longer-lasting smaller-amplitude rarefaction, well-described by the Friedlander equation (Marchetti et al., 2013). Shock waves at Volcán de Fuego are dominated by energy peaking in the 0.8–2 Hz band (**Figures 5A,B** and **Supplementary Material SM2 a**).

Figure 6A shows a record section plot for an explosion recorded across the 2018 temporary infrasound network with a peak overpressure of 370 Pa at 1 km from the source, on 19 May at 04:19:05 (UTC Time). The Mach number for this explosion was estimated to be 1.3, using procedures described by Marchetti et al. (2013). A propagation speed of 442 m/s is consistent with the infrasound onset at the closest station to the vent — VF03, 1 km from source — and reflects non-linear propagation of a shock-wave. The propagation speed between the vent and VF03 was estimated using the explosion onset time calculated from data recorded at all other stations in the network. Infrasound propagates at 330 m/s across the network beyond VF03 reflecting the transition between the supersonic and sonic regimes at greater distances from the vent (**figure 6A**). The event registered at 5.2 km from the vent (station VF04) also displays the characteristic N-shape, which is expected for shock waves that have propagated far from their source (Marchetti et al., 2013).

FIGURE 5 | Acoustic waveforms, spectra, and spectrograms of shock-wave **(A,B,C)**, gas-rich **(D,E,F)**, tephra-rich explosions **(G,H,I)**, and longer duration explosions **(J,K,L)**. Note differences in amplitude, duration, and spectral content between events.

Tephra-Rich Explosions

Tephra-rich explosions are recorded as symmetric transients with a longer (order of 10–15 s) and more complex coda (**Figure 5G**, and **Supplementary Material SM2 c**). Examples of these explosions have also been reported at Sakurajima, Japan (Matoza et al., 2014), Karymsky, Russia (Johnson and Malone, 2007; Lopez et al., 2013), and Tungurahua, Ecuador (Fee et al., 2010b), among other volcanoes. Tephra-rich explosions were dominant during November–December 2018, generally associated with lower recorded pressures. Field observations report dark plumes reaching 500–1,500 m above the vent.

Longer Duration Explosions

We also recorded explosive activity characterized by longer duration transients (order of 1–4 min) here referred to as longer duration explosions. These events are common at Volcán de Fuego, particularly during inter-paroxysm periods and effusive phases (**Figure 5J** and **Supplementary Material SM2 d**). Visual observations during these events describe turbulent plumes reaching 500–1,000 m above the vent and varying from light to dark gray depending on ash content (Field observations, **Supplementary Material SM 4**). The corresponding infrasound signature is characterized by low-amplitude emergent onsets followed by a long-lasting (1–4 min) low-frequency complex coda. Visual imagery (**Supplementary Material SM4**) of these events confirms the presence of multiple pulses at the vent, some more gas-rich (light

gray plume) and some more tephra-rich (dark-grey plume) being responsible for the long low-frequency coda in the infrasound record. On the other hand, turbulence of the plume might also play a role in shaping these complex signals (**Figures 5J,K,L**, and **Supplementary Material SM2 d**).

4.2. Harmonic and non-Harmonic Acoustic Tremor

Seismic tremor (ST) is a sustained-amplitude signal frequently observed at active volcanoes, commonly associated with magma ascent, surface degassing, lava fountains, and other eruption activity (McNutt, 1994; Chouet and Matoza, 2013). Recently, owing to development of volcano infrasound, observations of its acoustic counterpart have become commonplace; seismo-acoustic tremor (SAT) refers to the case in which the volcano radiates energy into both the ground and the atmosphere (Lees et al., 2004; Lesage et al., 2006; Lyons et al., 2013; Matoza et al., 2014). As for ST, SAT presents sub-types where the spectrum is dominated by multiple uncorrelated frequency peaks (broadband, SAT-BT) or by regularly spaced peaks (harmonic, SAT-HT), with consequent implications for its source mechanisms. Recently, Girona et al. (2019) modeled different types of tremor based on a conduit topped with a permeable cap setting and different gas flow regimes. BT was associated with random gas supply, while HT with periodic gas supply both with relatively thin caps (≤100 m).
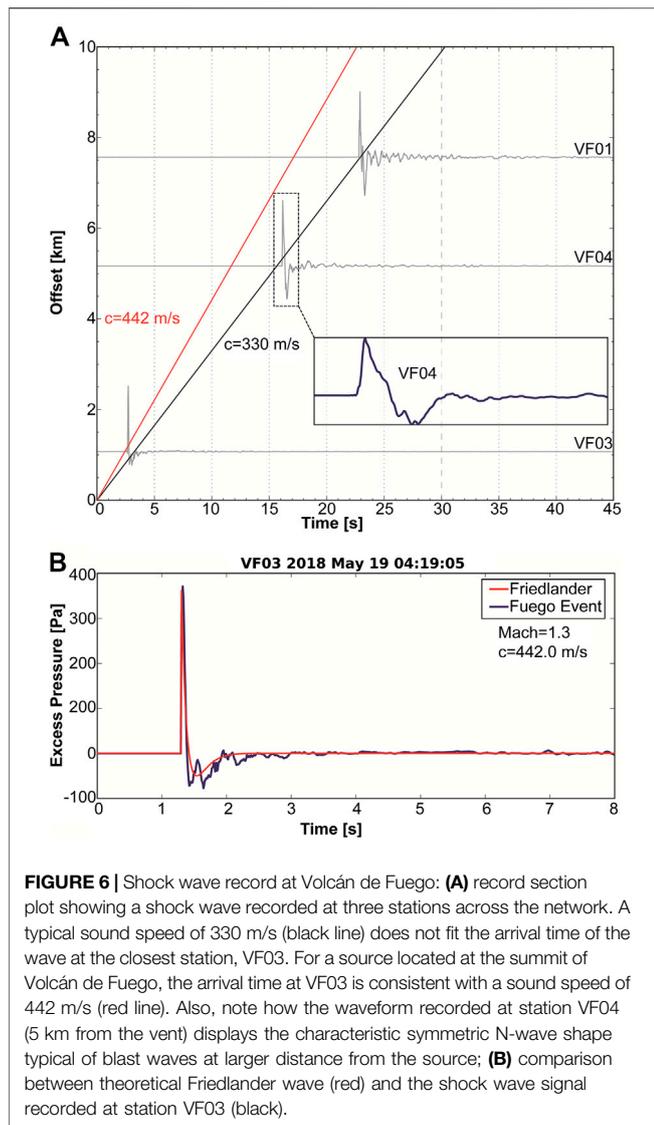
FIGURE 6 | Shock wave record at Volcán de Fuego: **(A)** record section plot showing a shock wave recorded at three stations across the network. A typical sound speed of 330 m/s (black line) does not fit the arrival time of the wave at the closest station, VF03. For a source located at the summit of Volcán de Fuego, the arrival time at VF03 is consistent with a sound speed of 442 m/s (red line). Also, note how the waveform recorded at station VF04 (5 km from the vent) displays the characteristic symmetric N-wave shape typical of blast waves at larger distance from the source; **(B)** comparison between theoretical Friedlander wave (red) and the shock wave signal recorded at station VF03 (black).

At Volcán de Fuego we recorded SAT, previously described by Lyons et al. (2013), with both broadband and harmonic signatures in May 2018. SAT was particularly intense starting on May 21, 2018, accompanying visible changes in eruptive activity, that shifted from discrete Strombolian explosions to sustained ash and gas emissions (**Figures 7,10**). In addition, we recorded characteristic form of quasi-periodic harmonic tremor referred to as "chugging". Chugging is a tremor-like signal that appears as a sequence of repeating explosions in rapid succession (**Figures 7C,8**). SAT-BT at Volcán de Fuego delivers energy between 0.5–8 Hz similar to the events described by Brill et al. (2018) (**Figure 7A**). Tremor episodes last between 1 and 60 min and were recorded during both campaigns in May and November 2018, although particularly intense during the second half of May (starting on the 21st). According to McNutt et al. (2015), SAT-BT can typically be associated with more vigorous and continuous ash and gas emissions. SAT-HT appears with non-stationary fundamental frequency between

1.5 and 2 Hz and three to six clear overtones (**Figure 7B**). SAT-HT episodes present similar duration as the SAT-BT and were more energetic during the last days of May. Both types of events (SAT-BT and SAT-HT) were clearly recorded at the closest station (VF03, 1 km from the vent) and still visible at the furthest stations (VF01, 7 km from the vent).
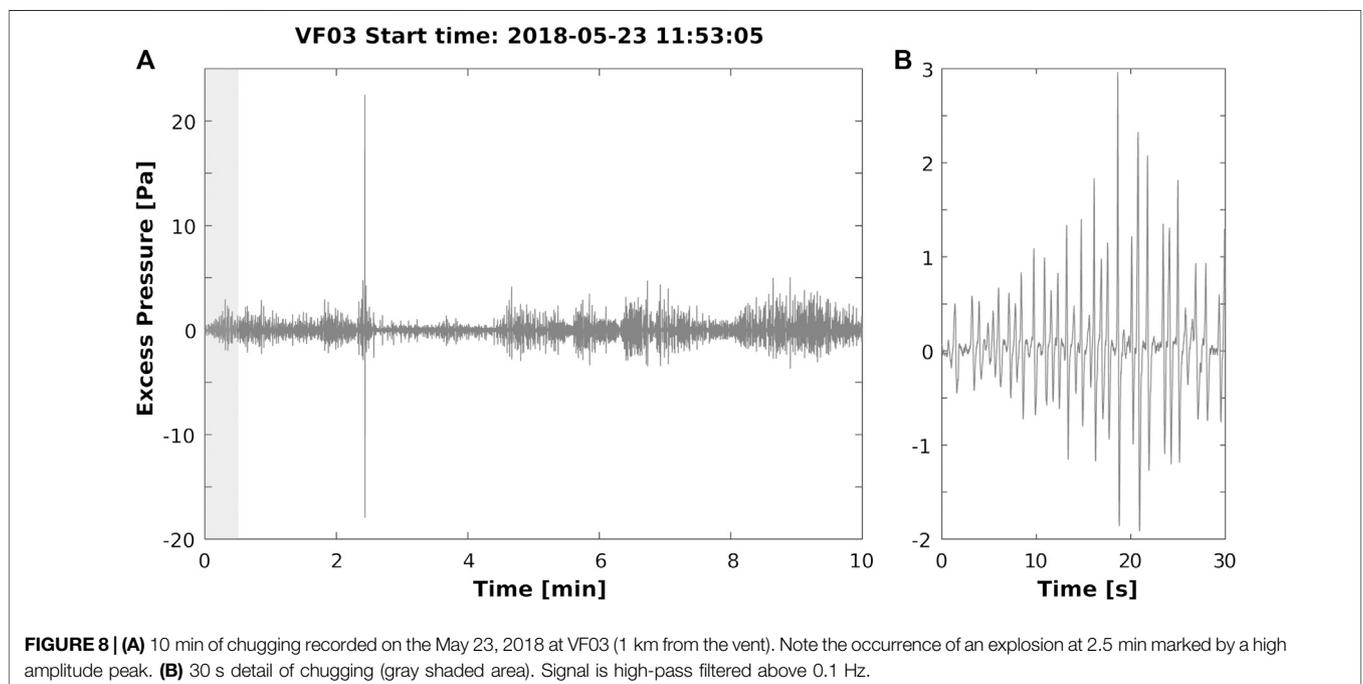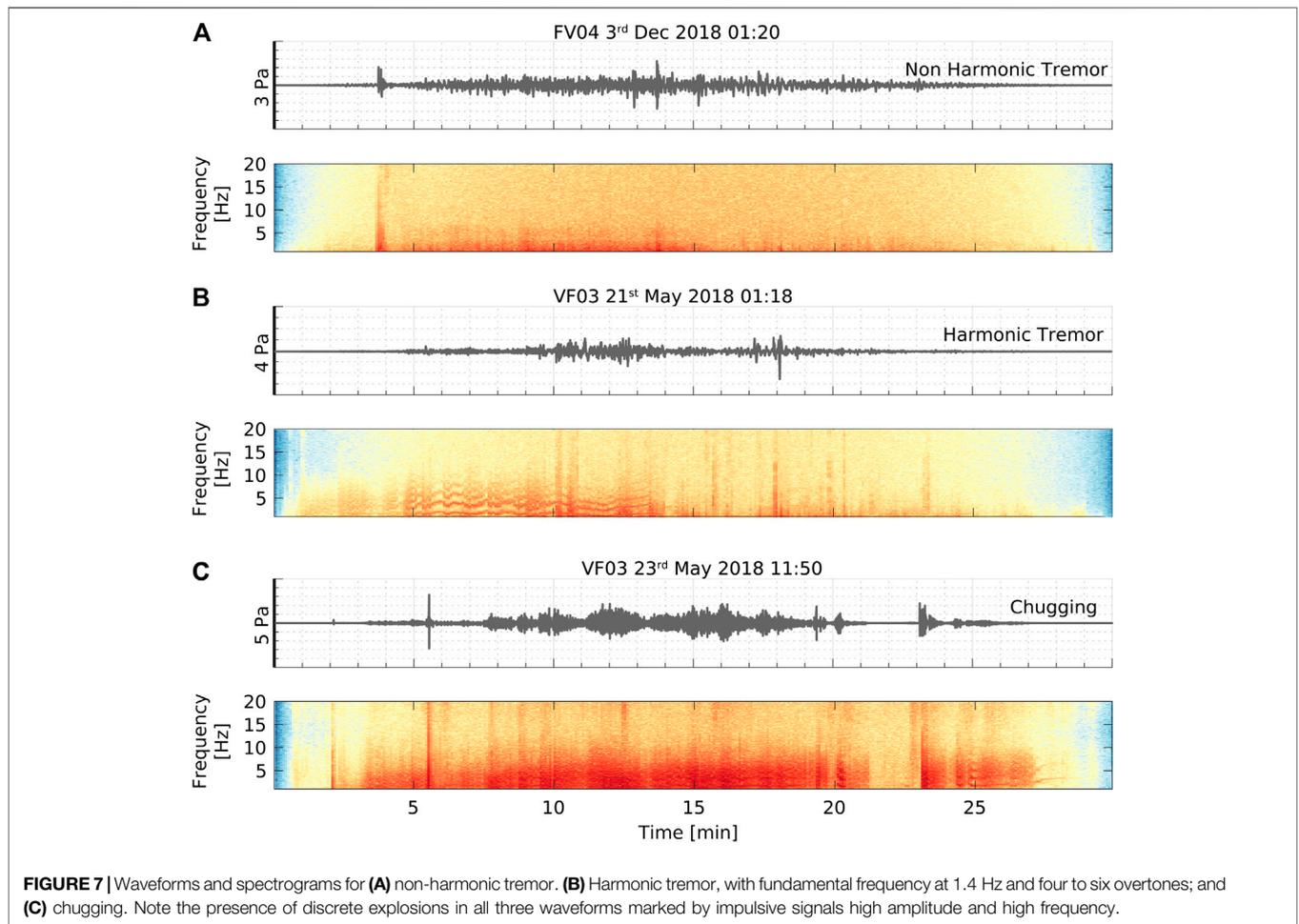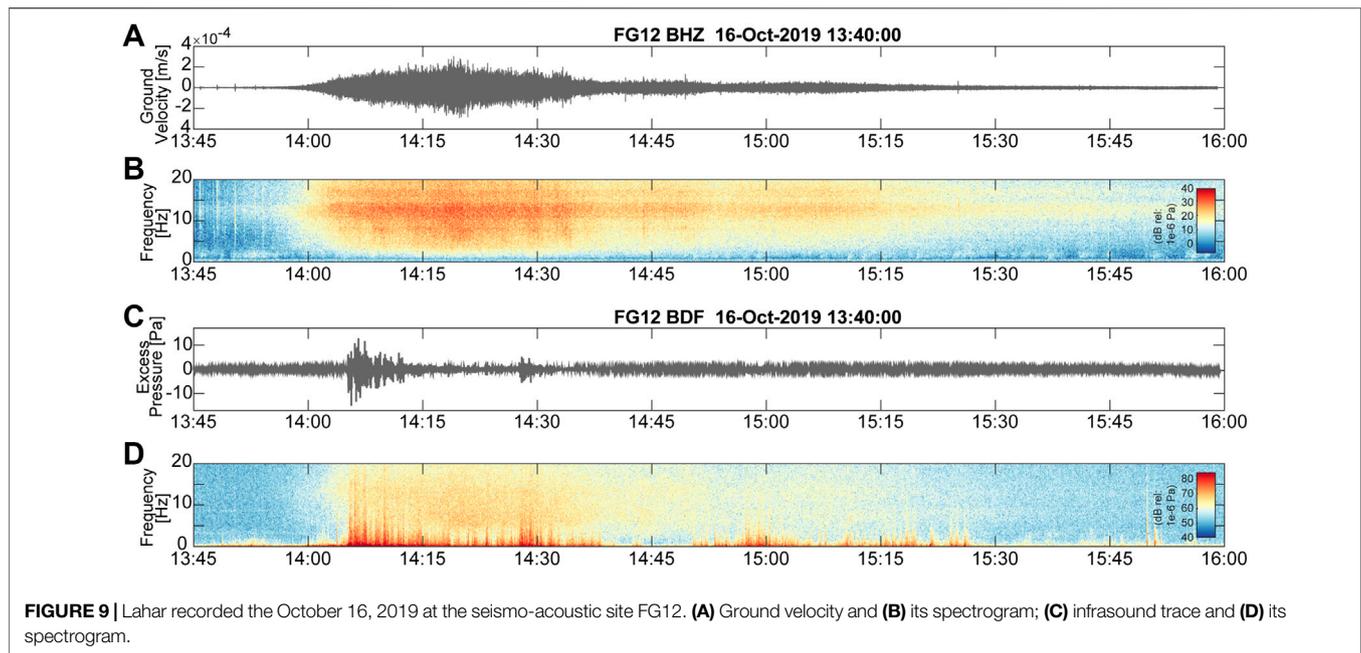
Chugging
Chugging waveforms resemble an amplitude modulated convolution between a simple base wavelet and a sequence of spikes, which would produce a quasi-harmonic spectrum (Lees and Ruiz, 2008). Examples of such signals have been reported in the past from Karymsky (Russia, Lopez et al., 2013)), Sangay (Ecuador, Johnson and Lees, 2000), Arenal (Costa Rica, Garcés and McNutt, 1997), Semeru (Indonesia, Schlindwein et al., 1995), Sabancaya (Peru, Ilanko et al., 2019) and Mt Etna (Italy, De Angelis et al., 2020), where chugging waveforms were associated with both pulsating degassing and vigorous repetitive Strombolian activity. In the literature, chugging associated with degassing explosions has been interpreted as resulting from the presence of a viscous plug at the vent acting as a valve over a pressurized system of volatiles and magma. The opening and closing of such a valve allows release of gas as a series of regular impulsive events (Lees and Bolton, 1998). At Volcán de Fuego, we recorded intense periods of acoustic chugging between 21 and May 23, 2018, associated with both strong pulsating degassing and frequent Strombolian explosions ejecting incandescent rock at heights of about 150–200 m above the vent (Visual observations by A. Lamur, May 2018). Episodes of chugging at Fuego last between 10 min and 1 h. In May 2018, we recorded peak infrasound amplitudes of about 3 Pa at 1 km from the vent (**Figures 7C,8** and **Supplementary Material SM2 g**). The appearance of this signal in May 2018 marked a clear transition in activity evolving from discrete Strombolian explosions to more sustained emissions and semi-continuous lava fountaining.

4.3. Lahars
Lahars (mud flows) are gravity-driven mixture of rock, debris, and water from a volcano (Vallance and Iverson, 2015). They are a frequent and major threat for population and infrastructure on the slopes of Volcán de Fuego. Lahars are triggered when rain interacts with pyroclastic deposits on the flanks of volcanoes (Thouret and Lavigne, 2000). These conditions are found at many volcanoes around the world and examples of the occurrence and, at times, catastrophic impacts of lahars are numerous: Nevado del Ruiz, Colombia (Lowe et al., 1986), Villarica, Chile (Johnson and Palma, 2015), Merapi, Indonesia (Lavigne et al., 2000b), Mayon, Philipines (Rodolfo and Arguden, 1991), among others.

At Volcán de Fuego, a regular rainy season combined with the significant volume of eruptive deposits on the flanks of the volcano, produce frequent lahars that can travel tens of kilometers down the steep-sided valleys (barrancas) affecting fluvial systems and disrupting communication and access to nearby villages (Naismith et al., 2019). The seismic and infrasonic signatures of lahars are characterized by complex waveforms lasting between tens of minutes up to several hours (Zobin, 2012; Buurman et al., 2013). The acoustic signal, at Fuego, is made up of large-amplitude, short-duration, pulses with energy

FIGURE 7 | Waveforms and spectrograms for **(A)** non-harmonic tremor. **(B)** Harmonic tremor, with fundamental frequency at 1.4 Hz and four to six overtones; and **(C)** chugging. Note the presence of discrete explosions in all three waveforms marked by impulsive signals high amplitude and high frequency.

FIGURE 8 | (A) 10 min of chugging recorded on the May 23, 2018 at VF03 (1 km from the vent). Note the occurrence of an explosion at 2.5 min marked by a high amplitude peak. **(B)** 30 s detail of chugging (gray shaded area). Signal is high-pass filtered above 0.1 Hz.

FIGURE 9 | Lahar recorded the October 16, 2019 at the seismo-acoustic site FG12. **(A)** Ground velocity and **(B)** its spectrogram; **(C)** infrasound trace and **(D)** its spectrogram.

dominantly in the 1–15 Hz frequency band. The seismic signal has a characteristic spindle-like appearance and delivers energy in the 5–20 Hz band (**Figures 9A,B**). The high-frequency pulses observed in lahar infrasound might be caused by lightnings and thunders evidencing the passage of thunderstorms. Other potential explanation for the high-frequency pulses is the impact of larger-size boulders on the channel bed as they are transported along by the bulk of the slurry of pyroclastic materials, debris and water (broadband part of the signal). At Volcán de Fuego, the recent deployment of the permanent seismo-acoustic network allows reliable detection of these events during the rainy season (**Figures 9A,B**).
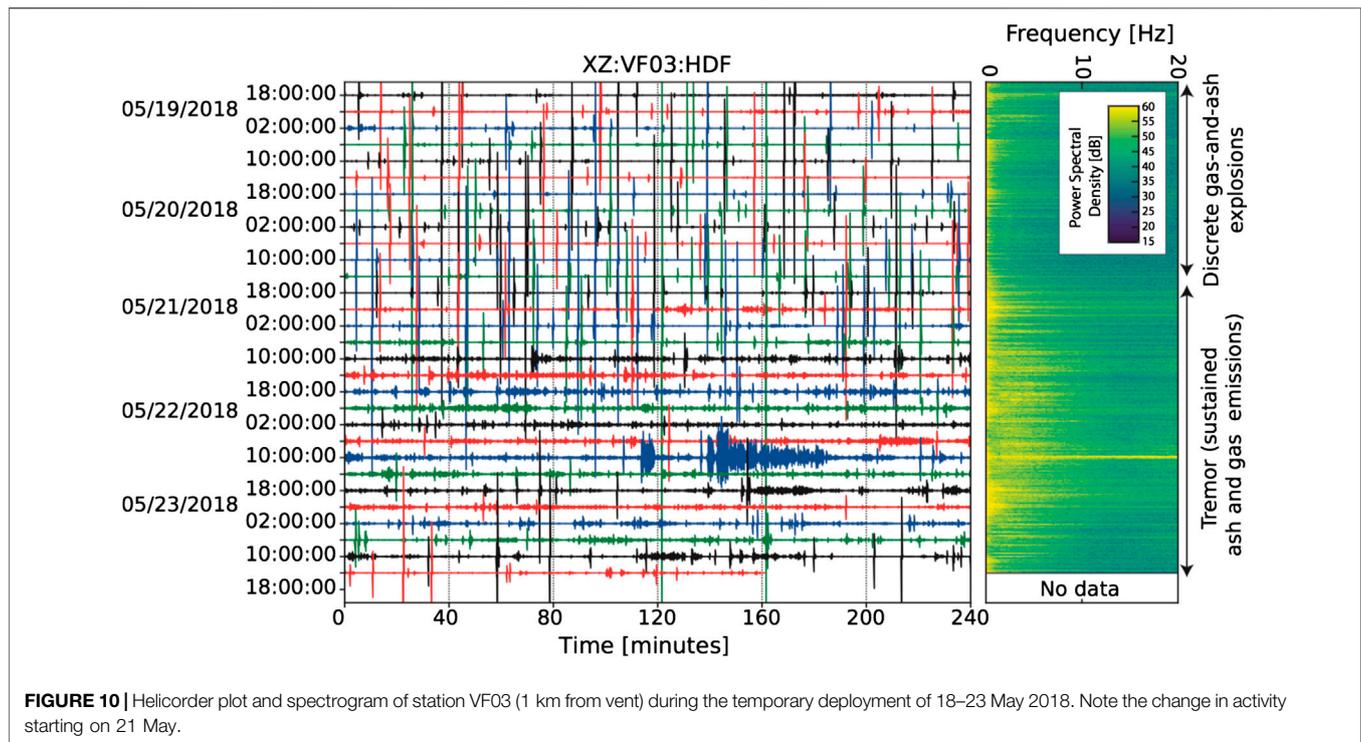
Timely detection of lahar onset is key to mitigating their hazard. The most common monitoring strategies range from human-observers (Tungurahua, Ecuador), to webcams (Sakurajima, Japan), and seismic monitoring (Merapi, Indonesia, Lavigne et al., 2000a; Hadley and LaHusen, 1995). At Volcán de Fuego, lahars represent a major threat for local communities and infrastructure, damaging farmlands and causing severe traffic disruptions, potentially isolating communities. Recently, many efforts have focused on monitoring and tracking their occurrence using seismo-acoustic arrays, which has proven a powerful tool for detecting, characterizing, and tracking sustained lahar activity.

5. DISCUSSION

5.1. Infrasound Signals and Monitoring

In this study we have presented the most common infrasound signals recorded at Volcán de Fuego. Discrete events range from pure gas-rich to tephra-rich explosions, with several intermediate types. Infrasound amplitudes range from several hundreds of Pa (measured at about 1 km from the vent) for gas-rich explosions

that generate shock waves, to tens of Pa for tephra-rich events (**Figure 5**). These types of signals typically coexist during periods between paroxysms. We also detect previously reported longer duration explosion with duration up to few minutes and smaller amplitudes **Figure 5**. We recorded a notable shift in eruptive activity from discrete and energetic gas-rich explosions to Strombolian-type explosions, then to sustained ash and gas emissions accompanied by quasi-continuous acoustic tremor on 21–23 May (**Figure 10**). This change in activity is translated to infrasound data as a marked increase in the overall amplitude and energy of the signal as illustrated by RSAM (Real-time seismic amplitude measurement) and spectrogram methods (**Figures 3,10**). A manually produced catalog with daily explosion counts and SAT-BT, SAT-HT, and chugging events and durations is provided for both experiments (**Supplementary Tables S1, S2**). We have observed two distinct vent configurations during the periods when these signals are recorded: a crater filled with lava forming an ephemeral cone with two or more active vents (**Figures 4A,B**), and an empty summit crater with explosions originating from a single vent (**Figures 4C,D**). It is clear, from observations reported in previous studies, that the presence of an ephemeral cone within the summit crater at Volcán de Fuego is mostly cyclical (Naismith et al., 2019). Conduit bifurcation during periods when an ephemeral cone is present has been associated with multiple vents within the crater area: a central vent predominantly characterized by Strombolian explosive activity, and a secondary one (or more) typically located on the flank of the ephemeral cone, associated with near-continuous degassing (Nadeau et al., 2011). Waite et al. (2013) observed and characterized different VLP events associated with sources linked to activity from both central and flank vents, remarking their importance in the explosions signature. Conduit

FIGURE 10 | Helicorder plot and spectrogram of station VF03 (1 km from vent) during the temporary deployment of 18–23 May 2018. Note the change in activity starting on 21 May.

bifurcation is particularly clear when an ephemeral cone is present within the summit crater (**Figures 4A,B**). In contrast, during periods when the crater is empty, a secondary vent is either not visible or less active (**Figures 4C,D**). From visual observations, we favor the presence of multiple vents as shallow features related to the presence of ephemeral unstable cones, where new sets of shallow fractures can be easily formed (Nadeau et al., 2011). The ephemeral cone might also play an important role in controlling the gas/ash ratio in the plumes; absence of the cone appears to favor gas-rich explosions with some ballistics, while its presence seems to be linked to larger quantities of ash in the plume (Patrick et al., 2007, **Figure 8**).

Unlike past observations, during our study period characterized by the presence two or more active vents, ash-, and gas-rich explosions occurred from all vents rather than preferentially at a given location (**Figure 4**). We suggest a model of conduit topped with a permeable plug and explosions linked to slug burst (Spina et al., 2019) underneath or within this viscous plug. Within the framework of this model explosion occurrence and intensity are controlled by the permeability of the upper conduit and ephemeral cone, and gas overpressure within the shallow conduit (Suckale et al., 2016; Barth et al., 2019). The characteristics of acoustic waveforms are controlled by the interaction of variable gas flow rates with the permeable plug. A numerical model recently presented by Girona et al. (2019) accounts for the presence of a viscous plug in the upper portions of the conduit and can accommodate all acoustics signals described in this manuscript. Similar models for explosion mechanisms have recently been proposed at Stromboli (Suckale et al., 2016;

Barth et al., 2019) and further tested with analogue and numerical modeling (Oppenheimer et al., 2019), and possibly through direct gas measurements (Pering et al., 2020).

5.2. Paroxysmal Activity

Paroxysms at Volcán de Fuego, similarly to other volcanoes, are eruptive episodes of rapid increase in the strength and occurrence of activity. During paroxysms, within the span of few hours, explosions rapidly increase in intensity and rates of occurrence, transitioning to semi-continuous explosive activity and eventually to sustained emission of pyroclastic materials from the vent. Several models have been proposed to explain the mechanisms involved in Volcán de Fuego's paroxysmal activity. Lyons et al. (2010), following two years of continuous observations at Volcán de Fuego (2005–2007), suggested two alternative models for explaining paroxysms: i) the collapsing foam model, originally proposed by Jaupart and Vergniolle (1988), where the accumulation and release of gas from an unstable foam layer are responsible for both effusive and explosive activity; and ii) rise-speed dependent model, introduced by Parfitt and Wilson (1995), where paroxysms are caused by higher rise-speeds of magma that prevent bubble coalescence and speed up fragmentation. In this latter model, lower rise-speeds would favor bubble coalescence into slugs, responsible for Strombolian activity. Both models can accommodate the observed cycles of lava effusion and mild strombolian explosions followed by paroxysmal eruptions and a final phase of discrete degassing explosions with no effusion. Building upon those models, rheological stiffening of basaltic and andesitic magmas in the upper portion of the conduit leads to a

plugged vent, below which gas accumulates before its periodic released (Johnson and Lees, 2000; Lyons and Waite, 2011). Moreover, the role of a permeable plug in generating common volcanic signals has been extensively investigated (Suckale et al., 2016; Barth et al., 2019; Girona et al., 2019).

A recent conceptual model for the trigger mechanism of paroxysms at Volcán de Fuego is introduced by Naismith et al. (2019), who supports the gravity-driven shedding of material from an ephemeral summit cone. According to these authors, an ephemeral cone is built up by fountaining ejected material and when the crater overspills, lava effusion begins. If the lava flow rate exceeds a certain threshold, the ephemeral cone might be destroyed, causing a depressurization of the system and thus trigger paroxysmal activity. Naismith et al. (2019) base their model on the presence of an ephemeral cone, which has been described in many eruptions at Volcán de Fuego (e.g., February 2017, October 2018) and acknowledge that it cannot explain episodes with no ephemeral cone (e.g., January 2016).

5.3. Long-Term Monitoring

Unfortunately, detailed long-term analyses of eruptive activity at Volcán de Fuego is limited by present data availability. Additional data would be required, for instance, to identify recurring patterns in the lead-up to paroxysms. Only one comparatively minor paroxysm has occurred since extensive and permanent geophysical monitoring of Volcán de Fuego was established in the summer of 2018. Geophysical data pre-2018 are limited to the temporary deployments mentioned in this manuscript. Available data from past deployments demonstrate consistent geophysical signatures for explosions at Volcan de Fuego over the past 10 years pointing to a rather stable and cyclic open-vent system. This evidence leaves us confident that, in the future, escalating activity leading to paroxysms could be detected by the newly established geophysical network. Data analyses from seismic and infrasound arrays have potential to underpin the development of alarm systems for Fuego, similar to present practice at other volcanoes such as Mt. Etna, Italy, (Ripepe et al., 2018; De Angelis et al., 2020), Alaskan volcanoes, USA, (Coombs et al., 2018; Power et al., 2020), and Soufrière Hills Volcano, Montserrat Island, (Thompson et al., 2020).

6. CONCLUSIVE REMARKS

We have presented and discussed the most common types of infrasound signals recorded at Volcán de Fuego during 2018-present. These range from discrete activity (including shock waves, gas-rich, and tephra-rich explosions) to more sustained emissions (seismo-acoustic broadband and harmonic tremor and chugging, and indirect volcanic processes as lahars).

We have reviewed previous acoustic studies at Volcán de Fuego. We have linked state-of-the-art numerical modeling available in literature to our gathered acoustic data. Data shown in this paper agree with recent models invoking the presence of a permeable plug on top of the magma column as a main feature controlling the infrasound signature of Volcán de Fuego.

We envision this work will serve as a baseline to interpret infrasound data recorded at Volcán de Fuego. Although infrasound is a valuable technique for volcano monitoring with robust workflows, we emphasize that effective volcano monitoring to support decision making and risk mitigation during eruptive crizes must include input from other disciplines such as seismology, gas geochemistry, and thermal remote sensing.

DATA AVAILABILITY STATEMENT

The datasets presented in this study can be found in online repositories. The names of the repository/repositories and accession number(s) can be found below: http://ds.iris.edu/mda/3E/?starttime=2018-01-01T00:00:00&endtime=2018-12-31T23:59:59.

AUTHOR CONTRIBUTIONS

All authors participated in the field experiments and contributed to the discussion of the manuscript. SA produced **Figures 2, 3**; AD produced all other figures with input from all co-authors; AD wrote the manuscript with input from all co-authors.

SUPPLEMENTARY MATERIAL

The Supplementary Material for this article can be found online at: https://www.frontiersin.org/articles/10.3389/feart.2020.549774/full#supplementary-material

REFERENCES

Barth, A., Edmonds, M., and Woods, A. (2019). Valve-like dynamics of gas flow through a packed crystal mush and cyclic strombolian explosions. *Sci. Rep.* 9, 821. doi:10.1038/s41598-018-37013-8

Berlo, K., Stix, J., Roggensack, K., and Ghaleb, B. (2012). A tale of two magmas, Fuego, Guatemala. *Bull. Volcanol.* 74, 377–390. doi:10.1007/s00445-011-0530-8

Brill, K. A., Waite, G. P., and Chigna, G. (2018). Foundations for forecasting: defining baseline seismicity at Fuego volcano, Guatemala. *Front. Earth Sci.* 6, 87. doi:10.3389/feart.2018.00087

Brogi, F., Ripepe, M., and Bonadonna, C. (2018). Lattice Boltzmann modeling to explain volcano acoustic source. *Sci. Rep.* 8, 9537. doi:10.1038/s41598-018-27387-0

Buurman, H., West, M. E., and Thompson, G. (2013). The seismicity of the 2009 Redoubt eruption. *J. Volcanol. Geotherm. Res.* 259, 16–30. doi:10.1016/J.JVOLGEORES.2012.04.024

Cannata, A., Hellweg, M., Di Grazia, G., Ford, S., Alparone, S., Gresta, S., et al. (2009a). Long period and very long period events at Mt. Etna volcano: characteristics, variability and causality, and implications for their sources. *J. Volcanol. Geotherm. Res.* 187, 227–249. doi:10.1016/j.jvolgeores.2009.09.007

Cannata, A., Montalto, P., Privitera, E., and Russo, G. (2009b). Characterization and location of infrasonic sources in active volcanoes: Mount Etna, September-November 2007. *J. Geophys. Res.: Solid Earth* 114, 1–15. doi:10.1029/2008JB006007

Chesner, C. A., and Rose, W. I. (1984). Geochemistry and evolution of the Fuego Volcanic complex, Guatemala. *J. Volcanol. Geotherm. Res.* 21, 25–44, doi:10.1016/0377-0273(84)90014-3

Chouet, B. A., and Matoza, R. S. (2013). A multi-decadal view of seismic methods for detecting precursors of magma movement and eruption. *J. Volcanol. Geotherm. Res.* 252, 108–175. doi:10.1016/j.jvolgeores.2012.11.013

Coombs, M. L., Wech, A. G., Haney, M. M., Lyons, J. J., Schneider, D. J., Schwaiger, H. F., et al. (2018). Short-term forecasting and detection of explosions during the 2016–2017 eruption of Bogoslof Volcano, Alaska. *Front. Earth Sci.* 6, 122. doi:10.3389/feart.2018.00122

De Angelis, S., Diaz-Moreno, A., and Zuccarello, L. (2019). Recent developments and applications of acoustic infrasound to monitor volcanic emissions. *Remote Sens.* 11, 1302. doi:10.3390/rs11111302

De Angelis, S., Fee, D., Haney, M., and Schneider, D. (2012). Detecting hidden volcanic explosions from Mt. Cleveland Volcano, Alaska with infrasound and ground-coupled airwaves. *Geophys. Res. Lett.* 39, L21312. doi:10.1029/2012GL053635

De Angelis, S., Haney, M., Lyons, J., Wech, A., Fee, D., Diaz-Moreno, A., et al. (2020). A simple framework to track the evolution of volcanic activity with infrasound arrays: examples from Mt. Etna, Italy. *Frontiers in Volcanology* (under rev). 8, 169. Available at: https://www.frontiersin.org/article/10.3389/feart.2020.00169. doi:10.3389/feart.2020.00169. ISSN: 2296-6463.

Deger, E. (1932). Der Ausbruch des Vulkans Fuego in Guatemala am 21 Januar 1932 und die chemische Zusammensetzung seiner Auswurfsmaterialien. *Chemie Der Erde* 7, 291–297.

Fee, D., and Garcés, M. (2007). Infrasonic tremor in the diffraction zone. *Geophys. Res. Lett.* 34, 1–5. doi:10.1029/2007GL030616

Fee, D., and Matoza, R. (2013). An overview of volcano infrasound: From Hawaiian to Plinian, local to global. *J. Volcanol. Geotherm. Res.* 249, 123–139. doi:10.1016/j.jvolgeores.2012.09.002

Fee, D., Garcés, M., Patrick, M., Chouet, B., Dawson, P., and Swanson, D. (2010a). Infrasonic harmonic tremor and degassing bursts from Halema'uma'u Crater, Kilauea Volcano, Hawaii. *J. Geophys. Res.: Solid Earth* 115, 1–15. doi:10.1029/2010JB007642

Fee, D., Steffke, A., and Garces, M. (2010b). Characterization of the 2008 Kasatochi and Okmok eruptions using remote infrasound arrays. *J. Geophys. Res.* 115, D00L10. doi:10.1029/2009JD013621

Ferrés, D. (2019). *Informe Técnico: Volcán de Fuego*. Mexico: Universidad Nacional Autónoma de México, 1–170.

Garcés, M. A., and McNutt, S. R. (1997). Theory of the airborne sound field generated in a resonant magma conduit. *J. Volcanol. Geotherm. Res.* 78, 155–178. doi:10.1016/S0377-0273(97)00018-8

Garcés, M., Fee, D., and Matoza, R. (2013). "Volcano Acoustics," in *Modeling volcanic processes: the physics and mathematics of volcanism*. Cambridge: Cambridge University Press.

Garcés, M., Fee, D., Steffke, A., McCormack, D., Servranckx, R., Bass, H., et al. (2008). Capturing the acoustic fingerprint of stratospheric ash injection. *Eos, Trans. AGU* 89, 377–378. doi:10.1029/2008EO400001

Girona, T., Caudron, C., and Huber, C. (2019). Origin of shallow volcanic tremor: the dynamics of gas pockets trapped beneath thin permeable media. *J. Geophys. Res.: Solid Earth* 124, 4831–4861. doi:10.1029/2019JB017482

Global Volcanism Program (2018a). Report on Fuego (Guatemala), 16 May-22 May 2018. Editor S. K. Sennert, Weekly Volcanic Activity Report, Smithsonian Institution and US Geological Survey

Global Volcanism Program (2018b). Report on Fuego (Guatemala), 21 November–27 November 2018. Editor S K Sennert, Weekly Volcanic Activity Report, Smithsonian Institution and US Geological Survey.

Global Volcanism Program (2018c). Report on Fuego (Guatemala), 30 May-5 June 2018. Editor S K Sennert, Weekly Volcanic Activity Report, Smithsonian Institution and US Geological Survey.

Grangeon, J., and Lesage, P. (2019). A robust, low-cost and well-calibrated infrasound sensor for volcano monitoring. *J. Volcanol. Geotherm. Res.* 387, 106668. doi:10.1016/J.JVOLGEORES.2019.106668

Hadley, K., and LaHusen, R. (1995). Technical manual for the experimental acoustic flow monitor (US Geological Survey).

Iezzi, A. M., Fee, D., Kim, K., Jolly, A., and Matoza, R. S. (2019). 3-D acoustic multipole waveform inversion at Yasur volcano, Vanuatu. *J. Geophys. Res.: Solid Earth* 124, 8679–8703. doi:10.1029/2018JB017073

Ilanko, T., Pering, T., Wilkes, T., Apaza Choquehuayta, F., Kern, C., Díaz Moreno, A., et al. (2019). Degassing at Sabancaya volcano measured by UV cameras and the NOVAC network. *Volcanica* 2, 239–252. doi:10.30909/vol.02.02.239252

Jaupart, C., and Vergniolle, S. (1988). Laboratory models of Hawaiian and Strombolian eruptions. *Nature* 331, 58–60. doi:10.1038/331058a0

Johnson, J. B. (2003). Generation and propagation of infrasonic airwaves from volcanic explosions. *J. Volcanol. Geotherm. Res.* 121, 1–14. doi:10.1016/S0377-0273(02)00408-0

Johnson, J. B., and Palma, J. L. (2015). Lahar infrasound associated with Volcán Villarrica's 3 March 2015 eruption. *Geophys. Res. Lett.* 42, 6324–6331. doi:10.1002/2015GL065024

Johnson, J. B., and Ripepe, M. (2011). Volcano infrasound: a review. *J. Volcanol. Geotherm. Res.* 206, 61–69. doi:10.1016/j.jvolgeores.2011.06.006

Johnson, J., and Lees, J. (2000). Plugs and chugs☐seismic and acoustic observations of degassing explosions at Karymsky, Russia and Sangay, Ecuador. *J. Volcanol. Geotherm. Res.* 101, 67–82. doi:10.1016/S0377-0273(00)00164-5

Johnson, J., and Malone, S. (2007). Ground-coupled acoustic airwaves from Mount St. Helens provide constraints on the May 18, 1980 eruption. *Earth Planet. Sci. Lett.* 1-2, 16–31. doi:10.1016/j.epsl.2007.03.001

Kamo, K., Ishihara, K., and Tahira, M. (1994). "Infrasonic and seismic detection of explosive eruptions at Sakurajima volcano, Japan, and the PEGASAS-VE early-warning system. in Proceedings of the First International Symposium on Volcanic Ash and Aviation Safety. Editor T. C. Casadevall, Seattle, Washington, July 1991. (Washington: United States Government Printing Office) (U.S. Geol. Surv. Bull.), Vol. 2047, 357–365

Lavigne, F., Thouret, J., Voight, B., Young, K., LaHusen, R., Marso, J., et al. (2000a). Instrumental lahar monitoring at Merapi Volcano, Central Java, Indonesia. *J. Volcanol. Geotherm. Res.* 100, 457–478. doi:10.1016%2FS0377-0273(00)00151-7

Lavigne, F., Thouret, J., Voight, B., Suwa, H., and Sumaryono, A. (2000b). Lahars at Merapi volcano, Central Java: an overview. *J. Volcanol. Geotherm. Res.* 100, 423–456. doi:10.1016%2FS0377-0273(00)00150-5

Lees, J., and Bolton, E. (1998). Pressure cookers as volcano analogues. *EOS, Trans. Am. Geophys. Union* 79, 45.

Lees, J. M., Gordeev, E. I., and Ripepe, M. (2004). Explosions and periodic tremor at Karymsky volcano, Kamchatka, Russia. *Geophys. J. Int.* 158, 1151–1167. doi:10.1111/j.1365-246X.2004.02239.x

Lees, J. M., and Ruiz, M. (2008). Non-linear explosion tremor at Sangay, Volcano, Ecuador. *J. Volcanol. Geotherm. Res.* 176, 170–178. doi:10.1016/j.jvolgeores.2007.08.012

Lesage, P., Mora, M. M., Alvarado, G. E., Pacheco, J., and Métaxian, J. P. (2006). Complex behavior and source model of the tremor at Arenal volcano, Costa Rica. *J. Volcanol. Geotherm. Res.* 157, 49–59. doi:10.1016/j.jvolgeores.2006.03.047

Lopez, T., Fee, D., Prata, F., and Dehn, J. (2013). Characterization and interpretation of volcanic activity at Karymsky Volcano, Kamchatka, Russia, using observations of infrasound, volcanic emissions, and thermal imagery. *Geochem., Geophys., Geosys.* 14, 5106–5127. doi:10.1002/2013GC004817

Lowe, D. R., Williams, S. N., Leigh, H., Connort, C. B., Gemmell, J. B., and Stoiber, R. E. (1986). Lahars initiated by the 13 November 1985 eruption of Nevado del Ruiz, Colombia. *Nature* 324, 51–53. doi:10.1038/324051a0

Lyons, J. J. (2011). *Dynamics and kinematics of eruptive activity at Fuego volcano , Guatemala 2005 – 2009*. Michigan: Michigan Technological University.

Lyons, J. J., Ichihara, M., Kurokawa, A., and Lees, J. M. (2013). Switching between seismic and seismo-acoustic harmonic tremor simulated in the laboratory:

Insights into the role of open degassing channels and magma viscosity. *J. Geophys. Res.: Solid Earth* 118, 277–289. doi:10.1002/jgrb.50067

Lyons, J. J., Iezzi, A. M., Fee, D., Schwaiger, H. F., Wech, A. G., and Haney, M. M. (2020). Infrasound generated by the 2016–2017 shallow submarine eruption of Bogoslof volcano, Alaska. *Bull. Volcanol.* 82, 19. doi:10.1007/s00445-019-1355-0

Lyons, J. J., and Waite, G. P. (2011). Dynamics of explosive volcanism at Fuego volcano imaged with very long period seismicity. *J. Geophys. Res.* 116, B09303. doi:10.1029/2011JB008521

Lyons, J. J., Waite, G. P., Rose, W. I., and Chigna, G. (2010). Patterns in open vent, strombolian behavior at Fuego volcano, Guatemala, 2005-2007. *Bull. Volcanol.* 72, 1–15. doi:10.1007/s00445-009-0305-7

Lyons, J. J., Waite, G. P., Ichihara, M., and Lees, J. M. (2012). Tilt prior to explosions and the effect of topography on ultra-long-period seismic records at Fuego volcano, Guatemala. *Geophys. Res. Lett.* 39. doi:10.1029/2012GL051184

Marchetti, E., Ripepe, M., Campus, P., Le Pichon, A., Brachet, N., Blanc, E., et al. (2019). "Infrasound monitoring of volcanic eruptions and contribution of ARISE to the Volcanic Ash Advisory Centers," in *Infrasound monitoring for atmospheric studies*. New York, NY: Springer International Publishing, 1141–1162.

Marchetti, E., Ripepe, M., Delle Donne, D., Genco, R., Finizola, A., and Garaebiti, E. (2013). Blast waves from violent explosive activity at Yasur Volcano, Vanuatu. *Geophys. Res. Lett.* 40, 5838–5843. doi:10.1002/2013GL057900

Marchetti, E., Ripepe, M., Ulivieri, G., Caffo, S., and Privitera, E. (2009). Infrasonic evidences for branched conduit dynamics at Mt. Etna volcano, Italy. *Geophys. Res. Lett.* 36, L19308. doi:10.1029/2009GL040070

Martin, D. P., and Rose, W. I. (1981). Behavioral patterns of Fuego volcano, Guatemala. *J. Volcanol. Geotherm. Res.* 10, 67–81. doi:10.1016/0377-0273(81)90055-X

Matoza, R., Arciniega-Ceballos, A., Sanderson, R., Mendo-Perez, G., Rosado-Fuentes, A., and Chouet, B. (2019a). High-broadband seismoacoustic signature of Vulcanian explosions at Popocatépetl volcano, Mexico. *Geophys. Res. Lett.* 46, 148–157. doi:10.1029/2018GL080802

Matoza, R., Fee, D., Green, D., and Mialle, P. (2019b). "Volcano Infrasound and the International Monitoring System," in *Infrasound monitoring for atmospheric studies*. New York, NY: Springer International Publishing, 1023–1077.

Matoza, R. S., Fee, D., Green, D. N., Le Pichon, A., Vergoz, J., Haney, M. M., et al. (2018). Local, regional, and remote seismo-acoustic observations of the April 2015 VEI 4 eruption of Calbuco Volcano, Chile. *J. Geophys. Res.: Solid Earth* 123, 3814–3827. doi:10.1002/2017JB015182

Matoza, R. S., Fee, D., and Lopez, T. M. (2014). Acoustic characterization of explosion complexity at Sakurajima, Karymsky, and Tungurahua Volcanoes. *Seismol Res. Lett.* 85, 1187–1199. doi:10.1785/0220140110

McNutt, S. R., Thompson, G., Johnson, J., Angelis, S. D., and Fee, D. (2015). "Chapter 63 - seismic and infrasonic monitoring," in *The encyclopedia of volcanoes*. 2nd Edn. Editor H. Sigurdsson (Amsterdam: Academic Press), 1071–1099.

McNutt, S. (1994). Volcanic tremor from around the world: 1992 update. *Acta Vulcanol.* 5, 197–200.

Nadeau, P. A., Palma, J. L., and Waite, G. P. (2011). Linking volcanic tremor, degassing, and eruption dynamics via SO2 imaging. *Geophys. Res. Lett.* 38. doi:10.1029/2010GL045820

Naismith, A. K., Matthew Watson, I., Escobar-Wolf, R., Chigna, G., Thomas, H., Coppola, D., et al. (2019). Eruption frequency patterns through time for the current (1999–2018) activity cycle at Volcán de Fuego derived from remote sensing data: Evidence for an accelerating cycle of explosive paroxysms and potential implications of eruptive activity. *J. Volcanol. Geotherm. Res.* 371, 206–219. doi:10.1016/J.JVOLGEORES.2019.01.001

Nishida, K., and Ichihara, M. (2016). Real-time infrasonic monitoring of the eruption at a remote island volcano using seismoacoustic cross correlation. *Geophys. J. Int.* 204, 748–752. doi:10.1093/gji/ggv478

Oppenheimer, J., Capponi, A., Cashman, K. V., Lane, S. J., Rust, A. C., and James, M. R. (2019). Analogue experiments on the rise of large bubbles through a solids-rich suspension : A " weak plug " model for Strombolian eruptions. *Earth Planet. Sci. Lett.* 1, 115931. doi:10.1016/j.epsl.2019.115931

Pallister, J., and McNutt, S. R. (2015). Synthesis of volcano monitoring. *The Encyclopedia of Volcanoes*, 1151–1171. doi:10.1016/B978-0-12-385938-9.00066-3

Pardini, F., Queißer, M., Naismith, A., Watson, I., Clarisse, L., and Burton, M. (2019). Initial constraints on triggering mechanisms of the eruption of Fuego volcano (Guatemala) from 3 June 2018 using IASI satellite data. *J. Volcanol. Geoth. Res.* 376, 54–61. doi:10.1016/J.JVOLGEORES.2019.03.014

Parfitt, E. A., and Wilson, L. (1995). Explosive volcanic eruptions-IX. The transition between Hawaiian-style lava fountaining and Strombolian explosive activity. *Geophys. J. Int.* 121, 226–232. doi:10.1111/j.1365-246X.1995.tb03523.x

Patrick, M. R., Harris, A. J., Ripepe, M., Dehn, J., Rothery, D. A., and Calvari, S. (2007). Strombolian explosive styles and source conditions: Insights from thermal (FLIR) video. *Bull. Volcanol.* 69, 769–784. doi:10.1007/s00445-006-0107-0

Pering, T., Liu, E., Wood, K., Wilkes, T., Aiuppa, A., Tamburello, G., et al. (2020). Combined ground and aerial measurements resolve vent-specific gas fluxes from a multi-vent volcanic system. *Nat. Commun.* 11, 3038. doi:10.1038%2Fs41467-020-16862-w

Power, J. A., Haney, M. M., Botnick, S. M., Dixon, J. P., Fee, D., Kaufman, A. M., et al. (2020). Goals and development of the Alaska volcano observatory seismic network and application to forecasting and detecting volcanic eruptions. *Seismol Res. Lett.* 91, 647–659. doi:10.1785/0220190216

Ripepe, M., and Marchetti, E. (2002). Array tracking of infrasonic sources at Stromboli volcano. *Geophys. Res. Lett.* 29, 33-1–33-4. doi:10.1029/2002GL015452

Ripepe, M., Marchetti, E., Delle Donne, D., Genco, R., Innocenti, L., Lacanna, G., et al. (2018). Infrasonic early warning system for explosive eruptions. *J. Geophys. Res.: Solid Earth* 123, 9570–9585. doi:10.1029/2018JB015561

Ripepe, M., and Marchetti, E. (2019). "Infrasound monitoring of volcano-related hazards for civil protection," in *Infrasound monitoring for atmospheric studies*. New York, NY: Springer International Publishing, 1107–1140

Rodolfo, K., and Arguden, A. (1991). "Rain-lahar generation and sediment delivery systems at Mayon Volcano, Philippines," in *Sedimentation in volcanic settings*. Tulsa, Oklahoma: SEPM Special Publication, Vol. 45.

Roggensack, K. (2001). Unraveling the 1974 eruption of Fuego volcano (Guatemala) with small crystals and their young melt inclusions. *Geology* 29, 911. doi:10.1130/0091-7613(2001)029□0911:UTEOFV□2.0.CO;2

Rose, W. I., Anderson, A. T., Woodruff, L. G., and Bonis, S. B. (1978). The october 1974 basaltic tephra from Fuego volcano: Description and history of the magma body. *J. Volcanol. Geoth. Res.* 4, 3–53. doi:10.1016/0377-0273(78)90027-6

Schlindwein, V., Wassermann, J., and Scherbaum, F. (1995). Spectral analysis of harmonic tremor signals at Mt. Semeru Volcano, Indonesia. *Geophys. Res. Lett.* 22, 1685–1688. doi:10.1029/95GL01433

Sisson, T., and Layne, G. (1993). H2O in basalt and basaltic andesite glass inclusions from four subduction-related volcanoes. *EarthPlanet. Sci. Lett.* 117 (3–4), 619–635. doi:10.1016/0012-821X(93)90107-K

Spina, L., Cannata, A., Morgavi, D., and Perugini, D. (2019). Degassing behaviour at basaltic volcanoes: new insights from experimental investigations of different conduit geometry and magma viscosity. *Earth-Sci. Rev.* 192, 317–336. doi:10.1016/j.earscirev.2019.03.010

Suckale, J., Keller, T., Cashman, K. V., and Persson, P. O. (2016). Flow-to-fracture transition in a volcanic mush plug may govern normal eruptions at Stromboli. *Geophys. Res. Lett.* 43, 12071–12081. doi:10.1002/2016GL071501

Taddeucci, J., Edmonds, M., Houghton, B., James, M. R., and Vergniolle, S. (2015). "Hawaiian and Strombolian Eruptions," in *The encyclopedia of volcanoes*. New York, NY: Elsevier, 485–503

Thompson, G., Power, J. A., Braunmiller, J., Lockhart, A. B., Lynch, L., Mccausland, W., et al. (2020). Capturing, preserving, and digitizing legacy seismic data from the montserrat volcano observatory analog seismic network. *Seismol Res. Lett.* 91, 2127–2140. doi:10.1785/0220200012

Thouret, J., and Lavigne, F. (2000). "Lahars: occurrence, deposits and behaviour of volcano-hydrologic flows," in *Volcaniclastic rocks from magma to sediments*. Amsterdam, The Netherlands: Gordon and Breach Science Publishers, 151–174

Tilling, R. I. (2008). The critical role of volcano monitoring in risk reduction. *Adv. Geosci.* 14, 3–11. doi:10.5194%2Fadgeo-14-3-2008

Vallance, J. W., and Iverson, R. M. (2015). "Lahars and Their Deposits," in *The Encyclopedia of Volcanoes*. 2nd Edn. New York, NY: Elsevier

Waite, G. P., Nadeau, P. A., and Lyons, J. J. (2013). Variability in eruption style and associated very long period events at Fuego volcano, Guatemala. *J. Geophys. Res.: Solid Earth* 118, 1526–1533. doi:10.1002/jgrb.50075

Walker, K. T., Hedlin, M. A. H., de Groot-Hedlin, C., Vergoz, J., Le Pichon, A., and Drob, D. P. (2010). Source location of the 19 February 2008 Oregon bolide using seismic networks and infrasound arrays. *J. Geophys. Res.* 115, B12329. doi:10.1029/2010JB007863

Wolf-Escobar, R. (2013). *Volcanic processes and human exposure as elements to build a risk model for Volcan de Fuego, Guatemala*. Michigan: Michigan Technological University.

Yuan, A. T. E., Mcnutt, S. R., and Harlow, D. H. (1984). Seismicity and eruptive activity at Fuego Volcano, Guatemala: February 1975–January 1977. *J. Volcanol. Geotherm. Res.* 21, 277–296. doi:10.1016/0377-0273(84)90026-X

Zobin, V. M. (2012). "Acoustic Waves Generated by Volcanic Eruptions," *in Introduction to Volcanic Seismology*, 381–406. Elsevier, London, UK.